

Competition between spin fluctuations in $\text{Ca}_{2-x}\text{Sr}_x\text{RuO}_4$ around $x = 0.5$

Naoya Arakawa* and Masao Ogata

Department of Physics, The University of Tokyo, Tokyo 113-0033, Japan

(Dated: April 27, 2022)

We study the static susceptibilities for charge and spin sectors in paramagnetic states for $\text{Ca}_{2-x}\text{Sr}_x\text{RuO}_4$ in $0.5 \leq x \leq 2$ within random phase approximation on the basis of an effective Ru t_{2g} orbital Hubbard model. We find that several modes of spin fluctuation around $\mathbf{q} = (0, 0)$ and $\mathbf{q} \sim (0.797\pi, 0)$ are strongly enhanced for the model of $x = 0.5$. This enhancement arises from the increase of the corresponding susceptibilities for the d_{xy} orbital due to the rotation-induced modifications of the electronic structure for this orbital (i.e., the flattening of the bandwidth and the increase of the density of states near the Fermi level). We also find that the ferromagnetic spin fluctuation becomes stronger for a special model than for the model of $x = 0.5$, while the competition between the modes of spin fluctuation at $\mathbf{q} = (0, 0)$ and around $\mathbf{q} \sim (\pi, 0)$ is weaker for the special model; in this special model, the van Hove singularity (vHs) for the d_{xy} orbital is located on the Fermi level. These results indicate that the location of the vHs for the d_{xy} orbital, which is controlled by substitution of Ca for Sr, is a parameter to control this competition. We propose that the spin fluctuations for the d_{xy} orbital around $\mathbf{q} = (0, 0)$ and $\mathbf{q} \sim (\pi, 0)$ play an important role in the electronic states around $x = 0.5$ other than the criticality approaching the usual Mott transition where all electrons are localized.

PACS numbers: 71.27.+a, 74.70.Pq

I. INTRODUCTION

$\text{Ca}_{2-x}\text{Sr}_x\text{RuO}_4$ is one of the strongly correlated electron systems with orbital degrees of freedom.^{1,2} This alloy has a quasi-two-dimensional crystalline structure, and the Ru t_{2g} orbitals and the lattice distortions induced by substitution of Ca for Sr play important roles in determining the electronic structures. Actually, this alloy shows a spin-triplet superconductivity,³⁻⁵ a heavy fermion (HF) behavior,⁶ and a metal-insulator transition,⁷ depending on the Sr concentration.

To clarify the origin of the HF behavior around $x = 0.5$, the present authors studied the electronic states for $\text{Ca}_{2-x}\text{Sr}_x\text{RuO}_4$ in $0.5 \leq x \leq 2$ within the Gutzwiller approximation on the basis of an effective Ru t_{2g} orbital Hubbard model;⁸ this effective model takes account of the change of the dp hybridizations due to the rotation of RuO_6 octahedra, which is induced in the range of $x < 1.5$. We proposed that this HF behavior can be qualitatively understood as the cooperative effect between moderately strong electron correlation and the orbital-dependent modification of the electronic structures due to the rotation of RuO_6 octahedra.⁸ In that study, however, we considered only the local correlations. It is thus needed to study the effects of the nonlocal correlation on the electronic structures, since both local and nonlocal correlations play important roles in discussing the electronic structure for a strongly correlated electron system in general.

In this paper, we study the static susceptibilities for charge and spin sectors in paramagnetic (PM) states for $\text{Ca}_{2-x}\text{Sr}_x\text{RuO}_4$ in $0.5 \leq x \leq 2$ within random phase approximation (RPA) on the basis of the effective Ru t_{2g} orbital Hubbard model.⁸ In particular, we analyze these static susceptibilities for the models of $x = 2$ and 0.5 ,

and a special model to clarify effects of the rotation of RuO_6 octahedra, the van Hove singularity (vHs) for the d_{xy} orbital, and the Hund's rule coupling. In this special model, the vHs for the d_{xy} orbital is located on the Fermi level.

The paper is organized as follows. In Sec. II, we first show the effective Ru t_{2g} orbital Hubbard model for $\text{Ca}_{2-x}\text{Sr}_x\text{RuO}_4$ in both the absence and the presence of the rotation of RuO_6 octahedra. Next, we introduce a generalized susceptibility for a multiorbital system and susceptibilities for charge and spin sectors. Then, we explain the method to determine a primary instability for a multiorbital system. In Sec. III, we first show the static susceptibilities and the maximum eigenvalues of static susceptibility for the models of $x = 2$ and 0.5 to analyze the effects of the rotation of RuO_6 octahedra. We next compare the results for the model of $x = 0.5$ with those for the special model to analyze the effects of the vHs for the d_{xy} orbital. Then, we show the dependence of the static susceptibilities on the Hund's rule coupling for the models of $x = 2$ and 0.5 , and the special model. In Sec. IV, we first address the mass enhancement due to the enhanced fluctuations for the models of $x = 2$ and 0.5 . In addition, we compare our results with previous theoretical and experimental works about magnetic properties. The paper concludes with a summary of our results in Sec. V.

II. FORMULATION

In the following, we set $\hbar = \mu_B = k_B = 1$, label the d_{xz} , d_{yz} , and d_{xy} orbitals as 1, 2, and 3, and choose the coordinates, x , y , and z , in the directions of the Ru-O bonds at $\phi = 0^\circ$ (i.e., $1.5 \leq x \leq 2$). Here, ϕ is an angle of the rotation of RuO_6 octahedra.

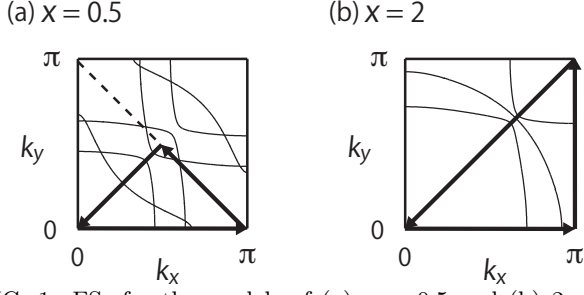


FIG. 1: FSs for the models of (a) $x = 0.5$ and (b) 2. The dashed line in Fig. (a) represents the folded BZ. The arrows in Figs. (a) and (b) correspond to the momentum lines used in the following figures.

To study the electronic states for $\text{Ca}_{2-x}\text{Sr}_x\text{RuO}_4$ in $0.5 \leq x \leq 2$, we consider an effective Ru t_{2g} orbital Hubbard model which takes account of the change of the dp hybridizations between the Ru $4d$ and O $2p$ orbitals due to the rotation of RuO_6 octahedra⁸:

$$\hat{H} = \hat{H}_0 + \hat{H}_{\text{int}}. \quad (1)$$

In the presence of the rotation of RuO_6 octahedra, the alternation of the direction of the rotation in the two-dimensional square lattice leads to a unit cell doubled, and the Brillouin zone (BZ) is folded [see Fig. 1 (a)].

The noninteracting Hamiltonian in the absence of the rotation of RuO_6 octahedra is given by

$$\hat{H}_0 = \sum_{\mathbf{k}} \sum_{a,b=1}^3 \sum_{s=\uparrow,\downarrow} \epsilon_{ab}(\mathbf{k}, 0^\circ) \hat{c}_{\mathbf{k}as}^\dagger \hat{c}_{\mathbf{k}bs}, \quad (2)$$

where $\epsilon_{ab}(\mathbf{k}, 0^\circ)$ denotes the energy dispersions for $\phi = 0^\circ$. These energy dispersions measuring from the chemical potential, μ , are given by

$$\epsilon_{11}(\mathbf{k}, 0^\circ) = -2t_1 \cos k_x - 2t_2 \cos k_y - \mu, \quad (3)$$

$$\epsilon_{12}(\mathbf{k}, 0^\circ) = \epsilon_{21}(\mathbf{k}, 0^\circ) = -4t' \sin k_x \sin k_y, \quad (4)$$

$$\epsilon_{22}(\mathbf{k}, 0^\circ) = -2t_2 \cos k_x - 2t_1 \cos k_y - \mu, \quad (5)$$

$$\epsilon_{33}(\mathbf{k}, 0^\circ) = -2t_3(\cos k_x + \cos k_y) - 4t_4 \cos k_x \cos k_y - \mu, \quad (6)$$

$$\epsilon_{ab}(\mathbf{k}, 0^\circ) = 0 \quad \text{otherwise}. \quad (7)$$

In this study, we take account of the next-nearest-neighbor (NNN) hopping integral between the d_{xz} and d_{yz} orbitals, which has been neglected in the previous study (Ref.8). μ is determined so that the total occupation number for the Ru t_{2g} orbitals is equal to 4.

For the model of $x = 2$, we set $t_1 = 0.675$, $t_2 = 0.09$, $t_3 = 0.45$, $t_4 = 0.18$, and $t' = 0.03$ so as to reproduce the experimentally observed Fermi surfaces (FSs).⁹ Here and throughout this paper, the energy unit is eV. Figure 1 (b) shows the FSs for this model. We see that the NNN hopping integral between the d_{xz} and d_{yz} orbitals leads to the slight change of the topology of the FS around $\mathbf{k} \sim (0.67\pi, 0.67\pi)$ from that without this NNN hopping integral (Ref.8); there are no qualitative changes in the density of states (DOS), which is not shown here.

In the presence of the rotation of the RuO_6 octahedra, the noninteracting Hamiltonian becomes

$$\hat{H}_0 = \sum_{\mathbf{k}} \sum_{a,b=1}^3 \sum_{l,l'=A,B} \sum_{s=\uparrow,\downarrow} \epsilon_{ab}^{ll'}(\mathbf{k}, \phi) \hat{c}_{\mathbf{k}als}^\dagger \hat{c}_{\mathbf{k}bl's}, \quad (8)$$

where the prime in the summation with respect to momentum represents the restriction within the folded BZ for $\phi \neq 0^\circ$, and l and $\epsilon_{ab}^{ll'}(\mathbf{k}, \phi)$ denote the sublattice index and the energy dispersions for $\phi \neq 0^\circ$. These energy dispersions measuring from μ are given by

$$\epsilon_{11}^{AA}(\mathbf{k}, \phi) = \epsilon_{22}^{AA}(\mathbf{k}, \phi) = \frac{1}{3} \Delta_{t_{2g}} - \mu, \quad (9)$$

$$\epsilon_{12}^{AA}(\mathbf{k}, \phi) = \epsilon_{21}^{AA}(\mathbf{k}, \phi) = -4t' \sin k_x \sin k_y, \quad (10)$$

$$\epsilon_{33}^{AA}(\mathbf{k}, \phi) = -\frac{2}{3} \Delta_{t_{2g}} - 4t_4 \cos k_x \cos k_y - \mu, \quad (11)$$

$$\epsilon_{11}^{AB}(\mathbf{k}, \phi) = -2t_1 \cos^2 \phi \cos k_x - 2(t_2 - t_1 \sin^2 \phi) \cos k_y, \quad (12)$$

$$\epsilon_{12}^{AB}(\mathbf{k}, \phi) = t_1 \sin 2\phi (\cos k_x + \cos k_y), \quad (13)$$

$$\epsilon_{21}^{AB}(\mathbf{k}, \phi) = -\epsilon_{12}^{AB}(\mathbf{k}, \phi), \quad (14)$$

$$\epsilon_{22}^{AB}(\mathbf{k}, \phi) = -2(t_2 - t_1 \sin^2 \phi) \cos k_x - 2t_1 \cos^2 \phi \cos k_y, \quad (15)$$

$$\begin{aligned} \epsilon_{33}^{AB}(\mathbf{k}, \phi) = & -2t_3 \cos^3 2\phi (\cos k_x + \cos k_y) \\ & + 2t_5 \cos 2\phi \sin^2 2\phi (\cos k_x + \cos k_y) \\ & - 4t_6 \cos 2\phi \sin^2 2\phi (\cos k_x - \cos k_y), \end{aligned} \quad (16)$$

$$\epsilon_{ab}^{AA}(\mathbf{k}, \phi) = \epsilon_{ab}^{AB}(\mathbf{k}, \phi) = 0 \quad \text{otherwise}, \quad (17)$$

$$\epsilon_{ab}^{BB}(\mathbf{k}, \phi) = \epsilon_{ab}^{AA}(\mathbf{k}, -\phi), \quad (18)$$

$$\epsilon_{ab}^{BA}(\mathbf{k}, \phi) = \epsilon_{ab}^{AB}(\mathbf{k}, -\phi). \quad (19)$$

The detail of the derivation of these energy dispersions is described in Ref. 8. In addition to the change of the hopping integrals due to the rotation of RuO_6 octahedra, we have taken account of the effect of the rotation-induced hybridization of the d_{xy} orbital to the $d_{x^2-y^2}$ orbital as the difference of the crystalline-electric-field (CEF) energies between the $d_{xz/yz}$ and d_{xy} orbitals, $\Delta_{t_{2g}}$.⁸

For the model of $x = 0.5$, we set $\phi = 15^\circ$, $\Delta_{t_{2g}} = 0.39$, and $t_5 = t_6 = 0$ so as to reproduce the experimentally observed FSs.¹⁰ Note that the value of $\Delta_{t_{2g}}$ in this study is different from that in the previous studies^{8,11} due to the introduction of the NNN hopping integral between the d_{xz} and d_{yz} orbitals. Figures 1 (a) and 2 show the FSs and DOS for this model. We see from Fig. 2 that the n.n.n. hopping integral between the d_{xz} and d_{yz} orbitals leads to a sharp decrease of the DOS for the d_{xz} and d_{yz} orbitals around an energy of -0.4 due to a small gap opening in the bands for these orbitals. This result is consistent with that obtained in the density-functional calculation for $x = 0.5$.¹²

In addition, to discuss the role of the vHs for the d_{xy} orbital, we consider the special model, for which we set $\phi = 15^\circ$, $\Delta_{t_{2g}} = 0.27$, and $t_5 = t_6 = 0$; similarly to the model of $x = 0.5$, the value of $\Delta_{t_{2g}}$ is different from that

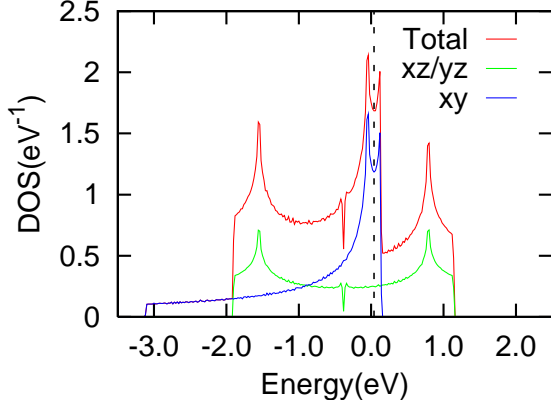


FIG. 2: (Color online) DOS for the model of $x = 0.5$. The dashed black line represents the chemical potential.

in the previous studies^{8,11}. In this special model, the vHs for the d_{xy} orbital is located on the Fermi level, as denoted in Sec. I.

We assume that the interacting Hamiltonian is given by the standard on-site interactions:

$$\begin{aligned} \hat{H}_{\text{int}} = & U \sum_j \sum_a \hat{n}_{ja\uparrow} \hat{n}_{ja\downarrow} + U' \sum_j \sum_{a>b} \hat{n}_{ja} \hat{n}_{jb} \\ & - J_H \sum_j \sum_{a>b} (2\hat{s}_{ja} \cdot \hat{s}_{jb} + \frac{1}{2} \hat{n}_{ja} \hat{n}_{jb}) \\ & + J' \sum_j \sum_{a>b} \hat{c}_{ja\uparrow}^\dagger \hat{c}_{ja\downarrow}^\dagger \hat{c}_{jb\downarrow} \hat{c}_{jb\uparrow}, \end{aligned} \quad (20)$$

where $\hat{n}_{ja} = \sum_s \hat{n}_{jas} = \sum_{s,s'} \hat{c}_{jas}^\dagger \sigma_{ss'}^0 \hat{c}_{jas'}$ and $\hat{s}_{ja} = \frac{1}{2} \sum_{s,s'} \hat{c}_{jas}^\dagger \boldsymbol{\sigma}_{ss'} \hat{c}_{jas'}$ with $\sigma_{ss'}^0$ and $\boldsymbol{\sigma}_{ss'}$ being the unit matrix and the Pauli matrices.

To analyze fluctuations for charge and spin sectors for a multiorbital system, we define a generalized susceptibility at temperature T as

$$\begin{aligned} & \chi_{as_1,bs_2;cs_3,ds_4}^{ll'}(\mathbf{q}, \tau) \\ & = \sum_{\mathbf{k}, \mathbf{k}'} \langle T_\tau \hat{c}_{\mathbf{k}'als_1}^\dagger(\tau) \hat{c}_{\mathbf{k}'+qbs_2}(\tau) \hat{c}_{\mathbf{k}cl's_3}^\dagger \hat{c}_{\mathbf{k}-qdl's_4} \rangle, \end{aligned} \quad (21)$$

and the corresponding Fourier coefficient is

$$\chi_{as_1,bs_2;cs_3,ds_4}^{ll'}(\mathbf{q}) = \int_0^{T^{-1}} d\tau e^{i\tau\Omega_n} \chi_{as_1,bs_2;cs_3,ds_4}^{ll'}(\mathbf{q}, \tau). \quad (22)$$

Here, T_τ is a chronological operator for imaginary time τ , $\hat{c}_{\mathbf{k}al\sigma}(\tau) = e^{\tau\hat{H}} \hat{c}_{\mathbf{k}al\sigma} e^{-\tau\hat{H}}$, and $q \equiv (\mathbf{q}, i\Omega_n)$ with Ω_n being a bosonic Matsubara frequency. In a PM state, the generalized susceptibility satisfies

$$\chi_{a\downarrow,b\downarrow;c\downarrow,d\downarrow}^{ll'}(\mathbf{q}) = \chi_{a\uparrow,b\uparrow;c\uparrow,d\uparrow}^{ll'}(\mathbf{q}), \quad (23)$$

$$\chi_{a\downarrow,b\uparrow;c\uparrow,d\downarrow}^{ll'}(\mathbf{q}) = \chi_{a\uparrow,b\downarrow;c\downarrow,d\uparrow}^{ll'}(\mathbf{q}). \quad (24)$$

The noninteracting susceptibility is

$$\chi_{abcd}^{ll'(0)}(\mathbf{q}) = -\frac{1}{TN} \sum_{\mathbf{k}} \sum_m G_{da}^{ll'(0)}(\mathbf{k} + \mathbf{q}) G_{bc}^{ll'(0)}(\mathbf{k}). \quad (25)$$

Here, $k \equiv (\mathbf{k}, i\omega_m)$ with ω_m being a fermionic Matsubara frequency, and $G_{ab}^{ll'(0)}(\mathbf{k})$ is the noninteracting Green's function:

$$G_{ab}^{ll'(0)}(\mathbf{k}) = \sum_{\alpha} (U_{\mathbf{k}})_{al;\alpha} \frac{1}{i\omega_m - \epsilon_{\alpha}(\mathbf{k}, \phi)} (U_{\mathbf{k}}^{\dagger})_{\alpha;bl'}, \quad (26)$$

where $(U_{\mathbf{k}})_{al;\alpha}$ is a unitary matrix to diagonalize \hat{H}_0 : $\hat{c}_{\mathbf{k}als} = \sum_{\alpha} (U_{\mathbf{k}})_{al;\alpha} \hat{c}_{\mathbf{k}\alpha s}$ and

$$\epsilon_{\alpha}(\mathbf{k}, \phi) = \sum_{a,b=1}^3 \sum_{l,l'=A,B} (U_{\mathbf{k}}^{\dagger})_{\alpha;al} \epsilon_{ab}^{ll'}(\mathbf{k}, \phi) (U_{\mathbf{k}})_{bl';\alpha}. \quad (27)$$

Let us introduce susceptibilities for charge and spin sectors as follows:

$$\chi_{abcd}^{ll'(C)}(\mathbf{q}) = \chi_{a\uparrow,b\uparrow;c\uparrow,d\uparrow}^{ll'}(\mathbf{q}) + \chi_{a\downarrow,b\downarrow;c\uparrow,d\uparrow}^{ll'}(\mathbf{q}), \quad (28)$$

$$\chi_{abcd}^{ll'(S)}(\mathbf{q}) = \chi_{a\uparrow,b\uparrow;c\uparrow,d\uparrow}^{ll'}(\mathbf{q}) - \chi_{a\downarrow,b\downarrow;c\uparrow,d\uparrow}^{ll'}(\mathbf{q}). \quad (29)$$

These susceptibilities characterize the fluctuations in a PM state since the spin-orbit interaction is neglected. For example, the fluctuation for spin degrees of freedom (i.e., spin fluctuation) is characterized by

$$\chi^S(\mathbf{q}) = \frac{1}{2} \sum_{l,l'=A,B} \sum_{a,b=1}^3 \chi_{aabb}^{ll'(S)}(\mathbf{q}), \quad (30)$$

where 1/2 is the normalization constant for the summation with respect to the sublattice indices.

$\chi_{abcd}^{ll'(C)}(\mathbf{q})$ and $\chi_{abcd}^{ll'(S)}(\mathbf{q})$ in Eqs. (28) and (29) are determined within the RPA by using the following equations:¹³⁻¹⁵

$$\chi_{abcd}^{ll'(C)}(\mathbf{q}) = \chi_{abcd}^{ll'(0)}(\mathbf{q}) + \sum_{\{a'\}} \sum_{l''} \chi_{aba'b'}^{ll''(0)}(\mathbf{q}) \Gamma_{a'b'c'd'}^C \chi_{c'd'cd}^{ll'(C)}(\mathbf{q}), \quad (31)$$

$$\chi_{abcd}^{ll'(S)}(\mathbf{q}) = \chi_{abcd}^{ll'(0)}(\mathbf{q}) + \sum_{\{a'\}} \sum_{l''} \chi_{aba'b'}^{ll''(0)}(\mathbf{q}) \Gamma_{a'b'c'd'}^S \chi_{c'd'cd}^{ll'(S)}(\mathbf{q}), \quad (32)$$

where $\sum_{\{a'\}} \equiv \sum_{a',b',c',d'}$ and the bare vertex interactions are

$$\Gamma_{abcd}^C = \begin{cases} -U & \text{for } a = b = c = d \\ -2U' + J_H & \text{for } a = b \neq c = d \\ U' - 2J_H & \text{for } a = d \neq b = c \\ -J' & \text{for } a = c \neq b = d \\ 0 & \text{otherwise} \end{cases}, \quad (33)$$

and

$$\Gamma_{abcd}^S = \begin{cases} U & \text{for } a = b = c = d \\ J_H & \text{for } a = b \neq c = d \\ U' & \text{for } a = d \neq b = c \\ J' & \text{for } a = c \neq b = d \\ 0 & \text{otherwise} \end{cases}, \quad (34)$$

respectively. These bare vertex interactions are independent of the sublattice indices since the interacting Hamiltonian (20) is diagonal in terms of these indices.

Since a phase transition is characterized by a divergence of static susceptibility, we calculate the eigenvalues of the static susceptibility by solving

$$\sum_{c,d} \sum_{l'} \chi_{abcd}^{l'(C)}(\mathbf{q}, 0) u_{cdl';\nu}^{(C)}(\mathbf{q}) = \lambda_{\nu}^C(\mathbf{q}) u_{abl;\nu}^{(C)}(\mathbf{q}), \quad (35)$$

$$\sum_{c,d} \sum_{l'} \chi_{abcd}^{l'(S)}(\mathbf{q}, 0) u_{cdl';\nu}^{(S)}(\mathbf{q}) = \lambda_{\nu}^S(\mathbf{q}) u_{abl;\nu}^{(S)}(\mathbf{q}). \quad (36)$$

Here, $\lambda_{\nu}^{C/S}(\mathbf{q})$ and $u_{abl;\nu}^{(C/S)}(\mathbf{q})$ are the eigenvalue of static susceptibility for a charge/spin sector and the corresponding eigenvector. We analyze the instability from the maximum eigenvalues:¹⁶

$$\lambda_{\max}^C(\mathbf{q}) = \max_{\nu} \left[\sum_{\{a\}} \sum_{l,l'} u_{\nu;abl}^{(C)\dagger}(\mathbf{q}) \chi_{abcd}^{l'(C)}(\mathbf{q}, 0) u_{cdl';\nu}^{(C)}(\mathbf{q}) \right], \quad (37)$$

$$\lambda_{\max}^S(\mathbf{q}) = \max_{\nu} \left[\sum_{\{a\}} \sum_{l,l'} u_{\nu;abl}^{(S)\dagger}(\mathbf{q}) \chi_{abcd}^{l'(S)}(\mathbf{q}, 0) u_{cdl';\nu}^{(S)}(\mathbf{q}) \right]. \quad (38)$$

Finally, to address the role of each Ru t_{2g} orbital in the fluctuations, we introduce the susceptibilities averaged with respect to the sublattice indices:

$$\chi_{abcd}^{(0)}(q) = \frac{1}{2} \sum_{l,l'=A,B} \chi_{abcd}^{l'(0)}(q), \quad (39)$$

$$\chi_{abcd}^{(C)}(q) = \frac{1}{2} \sum_{l,l'=A,B} \chi_{abcd}^{l'(C)}(q), \quad (40)$$

$$\chi_{abcd}^{(S)}(q) = \frac{1}{2} \sum_{l,l'=A,B} \chi_{abcd}^{l'(S)}(q). \quad (41)$$

III. RESULTS

In the following calculations, we set $T = 0.02$, $J' = J_H$, and $U' = U - 2J_H$, and use the values of U and J_H as parameters. To calculate the static susceptibilities, we divide the BZ into 128×128 meshes and take 1024 fermionic Matsubara frequencies for using the fast Fourier transformation.

A. Effects of the rotation of RuO₆ octahedra

To analyze the effects of the rotation of RuO₆ octahedra on the static susceptibilities, we compare the results for the model of $x = 2$ (i.e., $\phi = 0^\circ$) and 0.5 (i.e., $\phi = 15^\circ$).

First, the momentum dependencies of the noninteracting susceptibility for these models are shown in Figs. 3 (a) and (b). [Note that the momentum lines in both figures are along the arrows shown in Fig. 1 (b) to compare the cases of $x = 2$ and 0.5.] We find that the noninteracting susceptibility for the d_{xy} orbital around $\mathbf{q} = (0, 0)$ is larger for the model of $x = 0.5$ than for the model of

$x = 2$. This difference is due to the increase of the DOS for the d_{xy} orbital near the Fermi level in the presence of the rotation of RuO₆ octahedra.⁸ We also find that the incommensurate (IC) peaks for the $d_{xz/yz}$ orbital around $\mathbf{q} = (\pi, \pi)$ approach $\mathbf{q} = (\pi, \pi)$ as x is changed from 2 to 0.5; simultaneously, the IC peak for the d_{xy} orbital around $\mathbf{q} = (\pi, 0)$ approach $\mathbf{q} = (\pi, 0)$. These shifts are understood as follows: The rotation-induced hybridization of the d_{xy} orbital to the $d_{x^2-y^2}$ orbital leads to the downward shift of the energy level for the d_{xy} orbital.⁸ Correspondingly, the energy level for the $d_{xz/yz}$ orbital goes up compared with that for the d_{xy} orbital. The upward shift of the band for the $d_{xz/yz}$ orbital around $\mathbf{q} = (\pi, \pi)$ crossing the Fermi level leads to an increase of the nesting vector towards $\mathbf{q} = (\pi, \pi)$.

Next, we show the momentum dependencies of the maximum eigenvalue of static susceptibility in the RPA at $J_H = U/6$ for the models of $x = 2$ and 0.5. Figure 4 (a) shows the momentum dependencies of $\lambda_{\max}^S(\mathbf{q})^{-1}$ for the model of $x = 2$. We find that $\lambda_{\max}^S(\mathbf{q})^{-1}$ at $\mathbf{q} \sim (\pi, 0.5\pi)$ touches zero at $U = U_c = 0.975$, and that there are two main peaks at $\mathbf{q} \sim (\pi, 0.5\pi)$ and $(0.235\pi, 0.235\pi)$ and two secondary peaks at $\mathbf{q} \sim (\pi, 0.656\pi)$ and $(0.688\pi, 0.688\pi)$. Note that the enhancement of these main peaks is inconsistent with the experimental result of an inelastic neutron measurement,¹⁷ in which the enhancement of the IC antiferromagnetic (AF) spin fluctuation with $\mathbf{q} \sim (0.6\pi, 0.6\pi)$ is observed. However, as we will show below, our model can explain this experimental result. We also find that the increase of U leads to the suppression of the values of $\lambda_{\max}^C(\mathbf{q})^{-1}$ (not shown here).

It should be noted that the small value of U_c is due to the overestimation of the fluctuations in the RPA. This small value of U_c will be unrealistic since the value of U_c for transition metal oxides will be of the order of 2 – 3 eV. The similar problem remains for the model of $x = 0.5$ and the special model, as we will show below. In Sec. IV, we will address this problem and effects of the terms neglected in the RPA.

The momentum dependencies of $\lambda_{\max}^S(\mathbf{q})^{-1}$ for the model of $x = 0.5$ are shown in Fig. 4 (b); the inset represents $\lambda_{\max}^S(\mathbf{q})^{-1}$ at $U = U_c = 0.751$ in an expanded scale. [Hereafter, the momentum lines for $\phi \neq 0^\circ$ are along the arrows shown in Fig. 1 (a).] We find that $\lambda_{\max}^S(\mathbf{q})^{-1}$ at $\mathbf{q} = (0, 0)$ touches zero at $U = U_c = 0.751$, which is smaller than for the model of $x = 2$, and that there are two main peaks at $\mathbf{q} = (0, 0)$ and $\mathbf{q} \sim (0.797\pi)$ and a secondary peak at $\mathbf{q} \sim (\pi, 0.125\pi)$; all these peaks are less sharp than the peaks for the model of $x = 2$. As we will discuss in Sec. IV B, the enhancement of the main peak at $\mathbf{q} = (0, 0)$ is consistent with several experiments.^{18–20} We also find that the values of $\lambda_{\max}^C(\mathbf{q})^{-1}$ (not shown here) suppress as U increases. These results are qualitatively the same as those obtained in the previous study,¹¹ where the NNN hopping integral between the d_{xz} and d_{yz} orbitals has been neglected.

Moreover, Figs. 5 (a) and (b) show the momentum dependencies of $\chi_{aaaa}^{(S)}(\mathbf{q}, 0)$ in the RPA at $U = 0.8U_c$ for

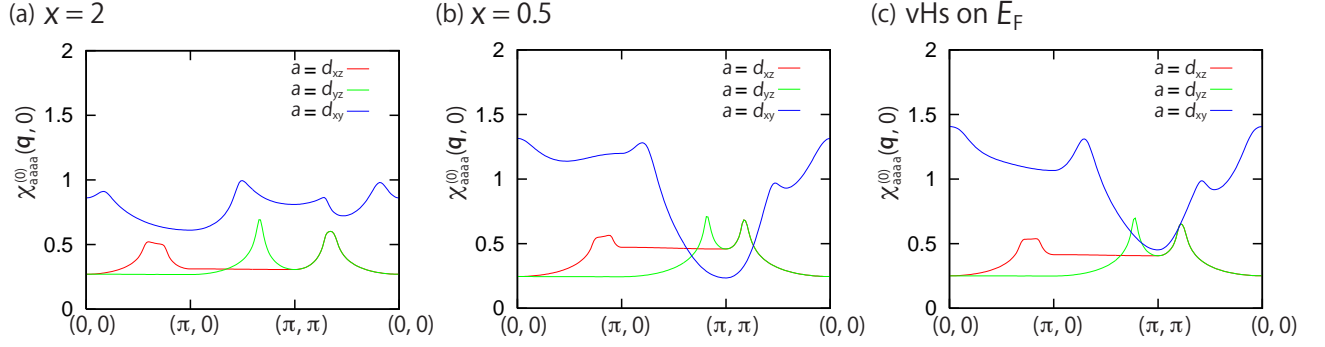


FIG. 3: (Color online) Momentum dependencies of $\chi_{aaaa}^{(0)}(\mathbf{q}, 0)$ for the models of (a) $x = 2$ and (b) 0.5, and (c) the special model.

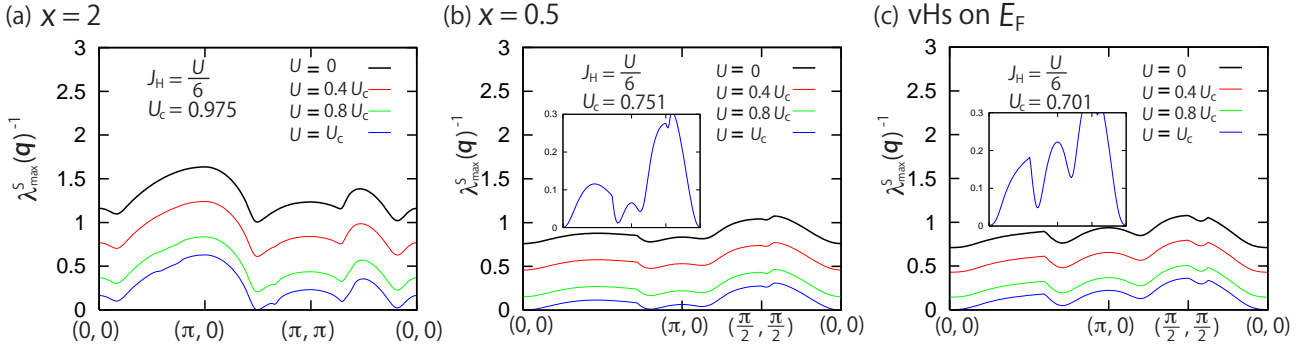


FIG. 4: (Color online) Momentum dependencies of $\lambda_{\max}^S(\mathbf{q})^{-1}$ in the RPA for the models of (a) $x = 2$ and (b) 0.5, and (c) the special model. The insets in (b) and (c) show the momentum dependencies of $\lambda_{\max}^S(\mathbf{q})^{-1}$ at $U = U_c$ in an expanded scale for the model of $x = 0.5$ and the special model, respectively.

the models of $x = 2$ and 0.5. For the model of $x = 2$, we see from Figs. 4 (a) and 5 (a) that the two main peaks in $\lambda_{\max}^S(\mathbf{q})^{-1}$ arise from the corresponding fluctuations for the d_{xy} orbital, and that the secondary peaks in $\lambda_{\max}^S(\mathbf{q})^{-1}$ at $\mathbf{q} \sim (\pi, 0.656\pi)$ and $(0.688\pi, 0.688\pi)$ arise from the corresponding fluctuation for the d_{yz} orbital and the combined fluctuation of the $d_{xz/yz}$ and d_{xy} orbitals. These results suggest that the fluctuations for a spin sector not only for the d_{xy} orbital but also for the $d_{xz/yz}$ orbital play an important role for $x = 2$.

For the model of $x = 0.5$, we see from Figs. 4 (b), 5 (b), and 6 (a) that the two main peaks and the secondary peak in $\lambda_{\max}^S(\mathbf{q})^{-1}$ arise from the corresponding fluctuations for the d_{xy} orbital, and that the contribution from the $d_{xz/yz}$ orbital is much smaller than for the d_{xy} orbital. Note that the value of $\chi_{aaaa}^{AA(S)}(\mathbf{q}, 0)$ for the d_{xy} orbital is about 10 times larger than for the $d_{xz/yz}$ orbital. These results suggest that the rotation of RuO_6 octahedra leads to the enhancement of several modes of spin fluctuation for the d_{xy} orbital around $\mathbf{q} = (0, 0)$ and $\mathbf{q} \sim (\pi, 0)$, and that the fluctuation for a spin sector for the d_{xy} orbital plays a more important role for $x = 0.5$ than for the $d_{xz/yz}$ orbital.

Finally, Figs. 7 (a) and (b) show the momentum dependencies of $\chi^S(\mathbf{q}, 0)$ in the RPA at $J_H = U/6$ for $U = 0.8U_c$ and $0.4U_c$ for the models of $x = 2$ and 0.5. For the

model of $x = 2$, we find from Fig. 7 (a) that $\chi^S(\mathbf{q}, 0)$ at $\mathbf{q} \sim (\pi, 0.5\pi)$, $(\pi, 0.656\pi)$, and $(0.688\pi, 0.688\pi)$ are dominant at $U = 0.8U_c$, while $\chi^S(\mathbf{q}, 0)$ at $\mathbf{q} \sim (0.688\pi, 0.688\pi)$ becomes largest at $U = 0.4U_c$; the main peak in $\lambda_{\max}^S(\mathbf{q})^{-1}$ at $\mathbf{q} \sim (0.235\pi, 0.235\pi)$ is less important at $U = 0.8U_c$ and $0.4U_c$. These results suggest that the experimentally observed enhancement¹⁷ of the IC AF spin fluctuation at $\mathbf{q} \sim (0.6\pi, 0.6\pi)$ can be understood if Sr_2RuO_4 is not located in the vicinity of the magnetic order. As we will show in Sec. III C, the Hund's rule coupling also plays an important role in enhancing this IC AF spin fluctuation.

For the model of $x = 0.5$, we find from Fig. 7 (b) that $\chi^S(\mathbf{q}, 0)$ at $\mathbf{q} = (0, 0)$ and $\mathbf{q} \sim (\pi, 0.125\pi)$ are dominant at $U = 0.8U_c$, while $\chi^S(\mathbf{q}, 0)$ at $\mathbf{q} = (0, 0)$, $\mathbf{q} \sim (0.797\pi, 0)$, and $(\pi, 0.125\pi)$ are nearly the same at $U = 0.4U_c$. Namely, almost all contributions arise from the corresponding fluctuations for the d_{xy} orbital. We also find that the values of $\chi^S(\mathbf{q}, 0)$ along $(0, 0) \rightarrow (\pi, 0)$ are larger than along $(0, 0) \rightarrow (\pi/2, \pi/2)$. This result indicates that the spin fluctuations along $(0, 0) \rightarrow (\pi, 0)$ are strongly enhanced for $x = 0.5$. This result is consistent with several inelastic neutron measurements,^{19,20} as we will address in Sec. IV B. These results suggest that the spin fluctuations for the d_{xy} orbital along $(0, 0) \rightarrow (\pi, 0)$ play a very important role for $x = 0.5$.

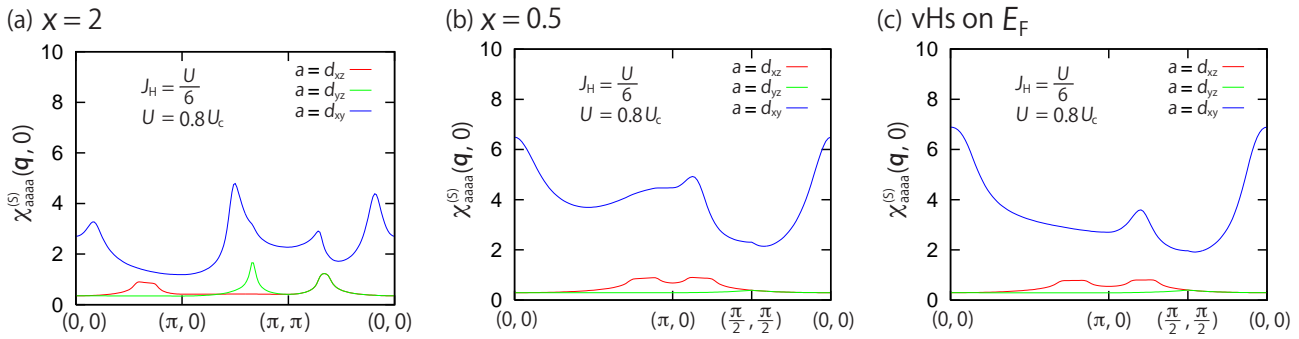


FIG. 5: (Color online) Momentum dependencies of $\chi_{aaaa}^{(S)}(\mathbf{q}, 0)$ in the RPA for the models of (a) $x = 2$ and (b) 0.5, and (c) the special model.

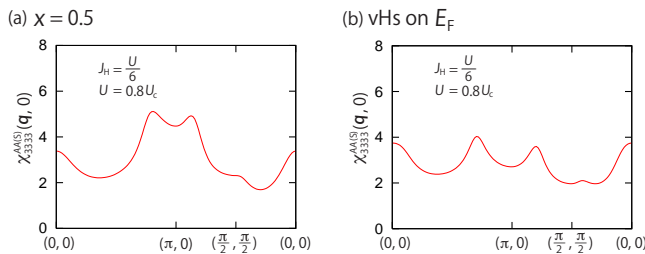


FIG. 6: (Color online) Momentum dependencies of $\chi_{aaaa}^{AA(S)}(\mathbf{q}, 0)$ for the d_{xy} orbital in the RPA for (a) the model of 0.5 and (b) the special model.

B. Effects of the vHs for the d_{xy} orbital

To analyze the effects of the vHs for the d_{xy} orbital on the static susceptibilities, we compare the results for the model of $x = 0.5$ with those for the special model, where the vHs is located on the Fermi level; the difference in these models is only the value of $\Delta_{t_{2g}}$.

First, the momentum dependence of the noninteracting susceptibility for the special model is shown in Fig. 3 (c). Comparing this figure with Fig. 3 (b), we see that the noninteracting susceptibility for the d_{xy} orbital around $\mathbf{q} = (0, 0)$ is larger for the special model than for the model of $x = 0.5$. This difference is due to the increase of the DOS for the d_{xy} orbital near the Fermi level in the special model. We also see that the shifts of the IC peak for the $d_{xz/yz}$ and d_{xy} orbitals, which are observed in the model of $x = 0.5$, are smaller in the special model. This difference arises from the smaller value of $\Delta_{t_{2g}}$ for the special model.

Next, Fig. 4 (c) shows the momentum dependencies of $\lambda_{\max}^S(\mathbf{q})^{-1}$ in the RPA at $J_H = U/6$ for the special model; the inset represents $\lambda_{\max}^S(\mathbf{q})^{-1}$ at $U = U_c = 0.701$ in an expanded scale. Comparing Fig. 4 (c) with Fig. 4 (b), we find that the value of U_c , where $\lambda_{\max}^S(\mathbf{q})^{-1}$ at $\mathbf{q} = (0, 0)$ touches zero, is smaller for the special model than for the model of $x = 0.5$, and that there is a main peak at $\mathbf{q} = (0, 0)$ and there is a secondary peak at $\mathbf{q} \sim (0.703\pi, 0)$; the latter peak corresponds to the peak at $\mathbf{q} \sim (0.797\pi, 0)$ for the model of $x = 0.5$. In addition, we see that all the peaks in $\lambda_{\max}^S(\mathbf{q})^{-1}$ for the

special model are slightly sharper than for the model of $x = 0.5$, and that the competition between the modes of spin fluctuation around $\mathbf{q} = (0, 0)$ and $\mathbf{q} \sim (\pi, 0)$ is weaker for the special model. The latter is due to the larger increase of the noninteracting susceptibilities for the d_{xy} orbital around $\mathbf{q} = (0, 0)$ compared with those around $\mathbf{q} \sim (\pi, 0)$ for the special model than for the model of $x = 0.5$. These results indicate that the location of the vHs for the d_{xy} orbital, which is controlled by substitution of Ca for Sr, is the parameter to control this competition. Note that the momentum dependencies of $\lambda_{\max}^C(\mathbf{q})^{-1}$ and $\chi_{aaaa}^C(\mathbf{q}, 0)$ (not shown) are qualitatively the same to those obtained for the model of $x = 0.5$.

Finally, Figs. 5 (c), 6 (b), and 7 (c) show the momentum dependencies of $\chi_{aaaa}^{(S)}(\mathbf{q}, 0)$, $\chi_{3333}^{AA(S)}(\mathbf{q}, 0)$, and $\chi^S(\mathbf{q}, 0)$ in the RPA for the special model. Comparing these figures with Figs. 5 (b), 6 (a), and 7 (b), we find the qualitatively same results to those for the model of $x = 0.5$. Namely, the enhanced modes in $\lambda_{\max}^S(\mathbf{q})^{-1}$ arise from the corresponding fluctuations for the d_{xy} orbital, and the dominant contributions to $\chi_{aaaa}^{(S)}(\mathbf{q}, 0)$ arise from those for the d_{xy} orbital around $\mathbf{q} = (0, 0)$ and $\mathbf{q} \sim (\pi, 0)$. These results suggest that the spin fluctuation for the d_{xy} orbital is more important in the electronic states around $x = 0.5$ than for the $d_{xz/yz}$ orbital.

C. Effects of the Hund's rule coupling

To analyze the effects of the Hund's rule coupling on the static susceptibilities, we compare the results in the RPA at $J_H = U/6$ with those at $J_H = 0$ and $U/4$.

First, we focus on the J_H dependence of the static susceptibilities for the model of $x = 2$. We find that the dominant wave vectors of these susceptibilities at $J_H = 0$ and $U/4$ (not shown) are same to those at $J_H = U/6$, and that the increase of J_H/U leads to the decrease of U_c . The latter is a typical behavior for a multiorbital system since the increase of J_H/U leads to an enhancement of spin fluctuations. We also find from Fig. 8 (a) that the static susceptibility for a charge sector is enhanced only at $J_H = 0$ as U increases. The similar enhancement has been reported in a RPA analy-

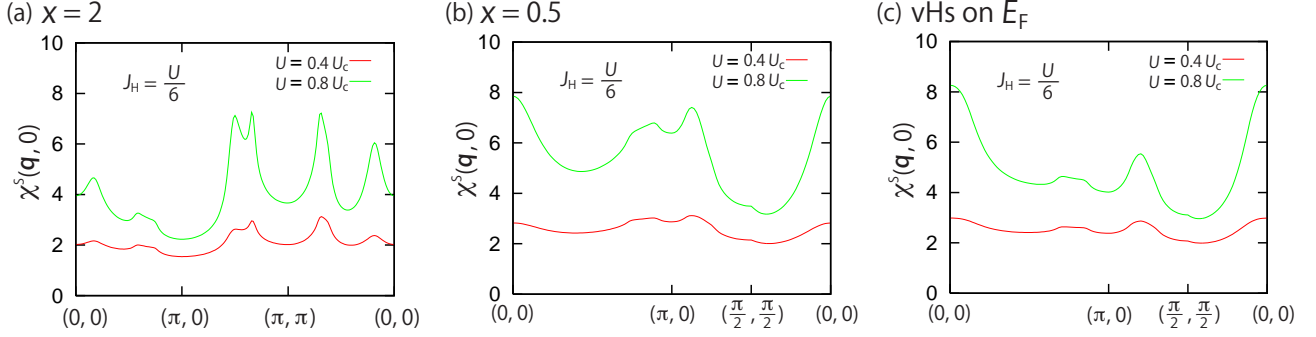


FIG. 7: (Color online) Momentum dependencies of $\chi^S(\mathbf{q}, 0)$ in the RPA for the models of (a) $x = 2$ and (b) 0.5, and (c) the special model.

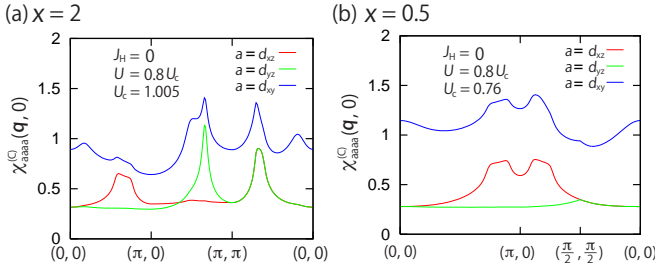


FIG. 8: (Color online) Momentum dependencies of $\chi^C_{aaaa}(\mathbf{q}, 0)$ in the RPA for the models of (a) $x = 2$ and (b) 0.5.

sis for $x = 2$,²¹ where the NNN hopping integral between the d_{xz} and d_{yz} orbitals has been neglected. Furthermore, we see from Fig. 9 (a) that $\chi^S(\mathbf{q}, 0)$ around $\mathbf{q} \sim (0.688\pi, 0.688\pi)$ and $(\pi, 0.656\pi)$ are strongly enhanced as J_H/U increases; these modes correspond to the secondary peaks in $\lambda^S_{\max}(\mathbf{q})^{-1}$ at $J_H = U/6$. The nature of these enhancements can be understood as follows:²² the Hund's rule coupling, which is one of the interorbital Coulomb interactions, more affects the orbitals having a finite hybridization.

Next, we turn to the J_H dependence of the static susceptibilities for the model of $x = 0.5$. Similarly to the case of $x = 2$, we find that the dominant wave vectors of the static susceptibilities at $J_H = 0$ and $U/4$ (not shown) are same to those at $J_H = U/6$, that the increase of J_H/U leads to the decrease of U_c , and that the increase of U leads to the enhancement of the static susceptibility for a charge sector only at $J_H = 0$ [see Fig. 8 (b)]. In contrast to the case of $x = 2$, we find from Fig. 9 (b) that the increase of J_H/U leads to a nearly uniform enhancement of $\chi^S(\mathbf{q}, 0)$; more precisely, the enhancement of $\chi^S(\mathbf{q}, 0)$ around $\mathbf{q} \sim (\pi, 0)$ is slightly larger than around $\mathbf{q} = (0, 0)$. This difference is due to the much larger contribution from the d_{xy} orbital for the model of $x = 0.5$ than from the $d_{xz/yz}$ orbital. These results indicate that the static susceptibilities for a spin sector for the d_{xy} orbital are very important for $x = 0.5$ regardless of the value of J_H/U .

Before showing the results for the special model, let us

remark on the effect of the rotation-induced hybridization of the d_{xy} orbital to the $d_{x^2-y^2}$ orbital on the J_H dependence of $\chi^S(\mathbf{q}, 0)$ for the model of $x = 0.5$. In this study, the effect of this hybridization is approximately taken account as the difference of the CEF energies between the $d_{xz/yz}$ and d_{xy} orbitals [see Eqs. (9) and (11)]. In principle, if this hybridization is fully taken into account, the J_H dependence of $\chi^S(\mathbf{q}, 0)$ will be modified. However, according to the density-functional calculation for $x = 0.5$,¹² the $d_{x^2-y^2}$ orbital has little weights to the bands near the Fermi level for $x = 0.5$. This result indicates that the values of the static susceptibility for the $d_{x^2-y^2}$ orbital are much smaller compared with those for the t_{2g} orbitals. Thus, the J_H dependence of $\chi^S(\mathbf{q}, 0)$ does not qualitatively change from the present result if this rotation-induced hybridization is fully taken into account.

Finally, we focus on the J_H dependence of the static susceptibilities for the special model. We find the similar J_H dependencies of the value of U_c and the static susceptibilities to those for the model of $x = 0.5$ [e.g., see Fig. 9 (c)]. Therefore, we conclude that the fluctuations for a spin sector for the d_{xy} orbital play a very important role in the electronic states around $x = 0.5$.

IV. DISCUSSION

We first address the mass enhancement due to the enhanced fluctuations for the models of $x = 2$ and 0.5. In this study, we find that the value of U_c is smaller for the model of $x = 0.5$ than for the model of $x = 2$, and that the peaks in $\lambda^S_{\max}(\mathbf{q})^{-1}$ are less sharp for the model of $x = 0.5$ [see Figs. 4 (a) and (b)]. In general, the effective mass at a certain value of U becomes large if the value of U_c is small.²³⁻²⁶ In addition, the effective mass becomes larger for a less sharp peak in the susceptibility, even if the value of the peak is same;²³⁻²⁶ this arises from the product of the susceptibility and the summation with respect to \mathbf{q} in the free energy. Combining these with our results, we conclude that the mass enhancement for the model of $x = 0.5$ will be much larger than for the model

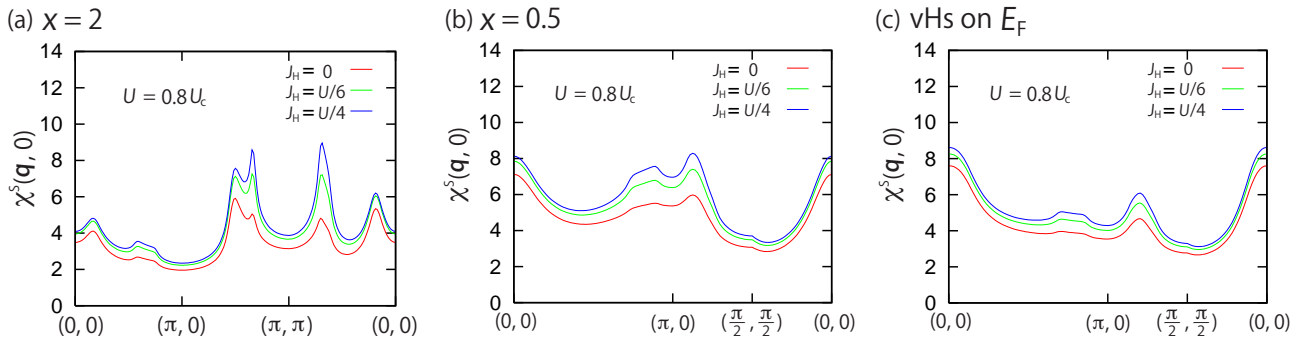


FIG. 9: (Color online) Momentum dependencies of $\chi^S(\mathbf{q}, 0)$ in the RPA for the models of (a) $x = 2$ and (b) $x = 0.5$, and (c) the special model.

of $x = 2$. Namely, we think that the present results can qualitatively explain the experimentally observed mass enhancement towards $x = 0.5$ (Ref.6); the actual calculation about the mass enhancement is a remaining future work.

A. Comparison with previous theoretical studies

We first compare our results with the previous theoretical studies about the magnetic properties for $\text{Ca}_{2-x}\text{Sr}_x\text{RuO}_4$ with $x = 2$. The mean-field calculation²² for $x = 2$ has found that the dominant contribution to the static susceptibility arises from that for the d_{xy} orbital. This calculation has also shown that the increase of J_H/U leads to the enhancement of the IC AF spin fluctuation around $\mathbf{q} \sim (0.67\pi, 0.67\pi)$, and that this IC AF spin fluctuation is strongest only for $J_H \geq U/2$ at $U = 1.25t_3 \sim 0.56$. Note that this mode of the enhanced IC AF spin fluctuation is different from $\mathbf{q} \sim (0.688\pi, 0.688\pi)$, which is enhanced in our study, due to the difference in the values of the hopping integrals. These results suggest that a moderately large Hund's rule coupling plays an important role for $x = 2$. This is consistent with the previous dynamical mean-field theory²⁷ for $x = 2$. Similarly to this mean-field study,²² we find that the increase of J_H/U leads to the enhancement of the IC AF spin fluctuations around $\mathbf{q} \sim (0.688\pi, 0.688\pi)$ and $(\pi, 0.656\pi)$; the former IC AF spin fluctuation is strongest for $J_H \geq U/6$ at $U = 0.8U_c \sim 0.78$. Since the enhancement of the IC AF spin fluctuation at $\mathbf{q} \sim (0.6\pi, 0.6\pi, 0)$ has been experimentally observed,¹⁷ we think that a set of the parameters used in this study is more realistic than in this previous mean-field study (Ref. 22).

Next, we address the physical meaning of the results obtained in the RPA, and compare our results with the studies in more elaborated treatments. The RPA is a mean-field-type approximation and neglects the mode-mode coupling for fluctuations. In general, the mode-mode coupling plays an important role in discussing the electronic states near a quantum critical point (QCP).²⁸⁻³¹ For example, it weakens the instability ob-

tained in the RPA. Actually, the previous study³² for $x = 2$ in fluctuation exchange (FLEX) approximation has observed much larger U_c than in the RPA; the FLEX approximation is partially taken account of the mode-mode coupling. We thus expect that the values of U_c will be more realistic than those obtained in this paper.

In addition to this, the mode-mode coupling can change the primary instability from that obtained in the RPA. Thus, the results about the primary instability may change when the mode-mode coupling is taken into account. Actually, the previous study³² for $x = 2$ in the FLEX approximation found that the IC AF spin fluctuation with $\mathbf{q} \sim (0.67\pi, 0.67\pi)$ is very strong, while the spin fluctuations with $\mathbf{q} \sim (\pi, 0.5\pi)$ and $(0.235\pi, 0.235\pi)$ are strongly enhanced in the RPA; the reason why this mode of the enhanced IC AF spin fluctuation in the FLEX is different from that in our study is the same as that for a case of the difference between the previous mean-field study²² and ours. However, we believe that the competition between the modes of spin fluctuation around $\mathbf{q} = (0, 0)$ and $\mathbf{q} \sim (\pi, 0)$ for the model of $x = 0.5$, which is obtained in this study, will not change even in a more elaborated treatment since the momentum dependence of $\lambda_{\max}^S(\mathbf{q})^{-1}$ is very flat; in such a case, it will be difficult that the mode-mode coupling favors a specific mode. Actually, our preliminary calculation³³ in the FLEX approximation observes the similar competition of spin fluctuations around these modes for the model of $x = 0.5$.

There are several density-functional calculations to study the ground states for $0.5 \leq x \leq 2$. Among them, a density-functional calculation within local-density approximation (LDA) has found that the rotation of RuO_6 octahedra enhances the ferromagnetic (FM) instability.³⁴ Another density-functional calculation³⁵ for $x = 0.5$ within the LDA has predicted the nesting instability with $\mathbf{q} \sim (0.29\pi, 0.29\pi, 0)$. The authors have proposed that this nesting instability will lead to the mass enhancement around $x = 0.5$; this nesting vector is related to a new FS induced by the rotation-induced hybridization of the d_{xy} orbital to the $d_{x^2-y^2}$ orbital. In our study, this new FS does not appear since we have not treated directly the rotation-induced hybridization of the d_{xy} orbital to the $d_{x^2-y^2}$ orbital; instead, we take account of the effect of

this hybridization as the difference of the CEF energies between the $d_{xz/yz}$ and d_{xy} orbitals, as denoted in Sec. II. In contrast to this density-functional calculation³⁵, another density-functional calculation for $x = 0.5$ within local spin-density approximation has found a disappearance of this nesting vector in the presence of the spin-orbit interaction, which is equal to 0.167 eV.¹² It is thus necessary to study the effects of this new FS on the electronic structures around $x = 0.5$ in more detail. However, we think that the presence of this new FS will not lead to the drastic changes from the present results since this rotation-induced FS is small and the DOS for each Ru t_{2g} orbital obtained in this study is almost the same as that obtained in these density-functional studies (Refs. 12 and 35).

Finally, we compare the obtained results with the previous study⁸ in the Gutzwiller approximation. This previous study calculated the total renormalization factor of the kinetic energy for the Ru t_{2g} orbitals, which is inversely proportional to the mass enhancement, and found that the inverse of the total renormalization factor is largest for the model of $x = 0.5$. Namely, these results can reproduce the experimentally observed tendency of the effective mass in $0.5 \leq x \leq 2$ (Ref. 6). These results suggest that the criticality approaching the usual Mott transition plays an important role in enhancing the effective mass towards $x = 0.5$; in this usual Mott insulator, the occupation numbers for the $d_{xz/yz}$ and d_{xy} orbitals are 1 and 2, respectively. On the other hand, in this study, we find that several modes of spin fluctuation for the d_{xy} orbital around $\mathbf{q} = (0, 0)$ and $\mathbf{q} \sim (0.797\pi, 0)$ are strongly enhanced for the model of $x = 0.5$. As discussed above, this enhancement of several modes will lead to the larger mass enhancement for $x = 0.5$ than for $x = 2$. This mechanism of the mass enhancement can coexist with the proposal in the previous study⁸ in the Gutzwiller approximation since the former and latter mass enhancements arise from the nonlocal and local effects. In other words, not only the criticality approaching the usual Mott transition, but also the spin fluctuations for the d_{xy} orbital around $\mathbf{q} = (0, 0)$ and $\mathbf{q} \sim (\pi, 0)$ play an important role in enhancing the effective mass towards $x = 0.5$.

B. Comparison with experimental results

We first address the correspondence of our results with several experimental results at $x = 2$. In addition to the inelastic neutron measurement,¹⁷ our results are consistent with the nuclear magnetic resonance (NMR) measurement.³⁶ This experiment has found that not only the IC AF spin fluctuation at $\mathbf{q} \sim (0.6\pi, 0.6\pi)$ but also the FM spin fluctuation plays the non-negligible role in enhancing the nuclear spin-lattice relaxation rate at a Ru site. This result indicates that the FM spin fluctuation also plays an important role in discussing the magnetic properties for $x = 2$. Actually, we see that the spin fluctuation around $\mathbf{q} = (0, 0)$ is non-negligible, although the

dominant components arise from the IC spin fluctuations around $\mathbf{q} \sim (\pi, 0.5\pi)$, $(0.235\pi, 0.235\pi)$, $(\pi, 0.656\pi)$, and $(0.688\pi, 0.688\pi)$.

Next, we compare our results with several experimental results in the presence of the rotation of RuO₆ octahedra. A recent muon spin relaxation (μ SR) measurement³⁷ for Ca_{2-x}Sr_xRuO₄ with $x = 0.5$ and 1.5 and Sr₂Ru_{1-y}Ti_yO₄ with $y = 0.09$ has shown that the muon relaxation rates rapidly increase as temperature decreases, and that the zero-field μ SR time spectra are similar to those for dilute-alloy spin glasses. The authors have proposed the static spin glass order not only in Sr₂Ru_{1-y}Ti_yO₄ but also in Ca_{2-x}Sr_xRuO₄ for $0.2 \leq x \leq 1.6$. However, all the previous experimental studies for Ca_{2-x}Sr_xRuO₄ in $0.5 \leq x \leq 2$ (Refs. 1,2,6,18–20,38,39) have suggested that the ground states are the PM metals. In addition, the elastic neutron measurement for $x = 1.5$ by the authors for this μ SR measurement has observed the absence of the ordered moment for $x = 1.5$, while the μ SR measurement has estimated the ordered moment at $0.25\mu_B$ per Ru. Therefore, we think that the conclusion for this μ SR measurement is doubtful, and that it is reasonable to analyze the static susceptibilities in the PM states to discuss the electronic states around $x = 0.5$.

We now discuss the correspondence with several neutron measurements. The polarized neutron diffraction measurement⁴⁰ for $x = 0.5$ has observed the anisotropic spin density distribution at a Ru site, which is flattened along c axis. This result suggests that the main part of the spin density arises from that for the d_{xy} orbital. Namely, the spin fluctuation for the d_{xy} orbital is predominant at $x = 0.5$. Actually, we find that the dominant contributions to the spin fluctuation arise from that for the d_{xy} orbital, which are consistent with this experimental result.

In addition to this neutron measurement, the inelastic neutron measurements^{19,20} for $x = 0.62$ have found that the FM scattering is maximum at an energy transfer of 0.4 meV, while the IC scatterings with $\mathbf{q} = (0.12, 0, 0)$ and $(0.27, 0, 0)$ evolve at an energy transfer of ~ 2.5 meV. These results indicate that the FM spin fluctuation is predominant at a lower energy transfer, while the IC spin fluctuations evolve as an energy transfer increases. Furthermore, these measurements^{19,20} have observed the intensity spreading in momentum space around the maximum peak and the large amplitude of the real part of the dynamic susceptibility at the maximum peak. These results indicate that several modes of spin fluctuation are more strongly enhanced for $x = 0.62$ than for $x = 2$, and that Ca_{2-x}Sr_xRuO₄ with $x = 0.62$ is located nearer to the boundary of the magnetic instability. Therefore, all the results for the model of $x = 0.5$ and the special model are qualitatively consistent with these experimental results except the evolution of the IC scatterings. It is necessary to study the origin of the evolution of these IC scatterings.

Our result for the model of $x = 0.5$ is also consistent

with the NMR measurement,¹⁸ in which the evolution of the FM spin fluctuation has been observed towards $x = 0.5$. This result of the NMR measurement is consistent with the dependence of the Wilson ratio on the Sr concentration.⁶

We now briefly remark on the metamagnetic transition observed for $\text{Ca}_{2-x}\text{Sr}_x\text{RuO}_4$ in the range of $0.2 \leq x \leq 0.5$.^{6,41} In this study, we focus on the electronic states for $0.5 \leq x \leq 2$ only in the absence of the external magnetic field. It is necessary to study the effects of the external magnetic field on the fluctuations for charge and spin sectors; this issue is a remaining future work.

Finally, we remark on the Curie-Weiss (CW) behavior in the spin susceptibility with a Curie constant corresponding to nearly $S = 1/2$ for $0.5 \leq x < 2$.^{1,2} The origin of this CW behavior has not been clarified yet. In general, there are two mechanisms in emerging the CW-type temperature dependence in the spin susceptibility.^{30,31} One is due to the formation of the localized moment, and the other is due to the drastic renormalization of the temperature dependence for the free energy by enhanced fluctuations. In the latter mechanism, the mode-mode coupling leads to this drastic renormalization.^{28,29} The emergence of the CW behavior in $\text{Ca}_{2-x}\text{Sr}_x\text{RuO}_4$ will arise from the latter mechanism since all electrons for the Ru t_{2g} orbitals are itinerant in $0.5 \leq x \leq 2$.^{10,42} In addition, we find for the model of $x = 0.5$ that several modes of spin fluctuation for the d_{xy} orbital around $\mathbf{q} = (0, 0)$ and $\mathbf{q} \sim (0.797\pi, 0)$ are strongly enhanced, and that the dominant contributions to the susceptibilities for a spin sector arise from those for the d_{xy} orbital. Therefore, we think that the mode-mode coupling for the d_{xy} orbital will play a more important role in discussing the spin susceptibility around $x = 0.5$ than for the $d_{xz/yz}$ orbital. It is necessary to study the electronic states around $x = 0.5$ on the basis of the microscopic theory taking account of the mode-mode coupling.

V. SUMMARY

To clarify the effects of the nonlocal (but not long-range) correlation on the electronic structures in $\text{Ca}_{2-x}\text{Sr}_x\text{RuO}_4$ around $x = 0.5$, we studied the static susceptibilities for charge and spin sectors in the PM states within the RPA for the models of $x = 2$ and 0.5 , and a special model. In particular, we analyzed the effects of the rotation of RuO_6 octahedra, the vHs for the d_{xy} orbital, and the Hund's rule coupling on these static susceptibilities.

First, we analyzed the effects of the rotation of RuO_6 octahedra by comparing the results at $J_H = U/6$ for the models of $x = 2$ and 0.5 . In the absence of interactions, we found that the rotation of RuO_6 octahedra leads to the increase of the noninteracting susceptibility for the d_{xy} orbital around $\mathbf{q} = (0, 0)$ and the shifts of the IC peak for the $d_{xz/yz}$ and d_{xy} orbitals towards $\mathbf{q} = (\pi, \pi)$ and $(\pi, 0)$. For the model of $x = 2$ in the RPA, we

found that $\lambda_{\text{max}}^{\text{S}}(\mathbf{q})^{-1}$ at $\mathbf{q} \sim (\pi, 0.5\pi)$ touches zero at $U = U_c = 0.975$, and that there are two main peaks in $\lambda_{\text{max}}^{\text{S}}(\mathbf{q})^{-1}$ at $\mathbf{q} \sim (\pi, 0.5\pi)$ and $(0.235\pi, 0.235\pi)$ and two secondary peaks at $\mathbf{q} \sim (\pi, 0.656\pi)$ and $(0.688\pi, 0.688\pi)$. The two main peaks arise from the corresponding fluctuations for the d_{xy} orbital, and the secondary peaks at $\mathbf{q} \sim (\pi, 0.656\pi)$ and $(0.688\pi, 0.688\pi)$ arise from the corresponding fluctuation for the d_{yz} orbital and the combined fluctuation of the $d_{xz/yz}$ and d_{xy} orbitals. We also found that $\chi^{\text{S}}(\mathbf{q}, 0)$ with $\mathbf{q} \sim (\pi, 0.5\pi)$, $(\pi, 0.656\pi)$, and $(0.688\pi, 0.688\pi)$ are dominant at $U = 0.8U_c$, while $\chi^{\text{S}}(\mathbf{q}, 0)$ with $\mathbf{q} \sim (0.688\pi, 0.688\pi)$ becomes largest at $U = 0.4U_c$. The main peak in $\lambda_{\text{max}}^{\text{S}}(\mathbf{q})^{-1}$ at $\mathbf{q} \sim (0.235\pi, 0.235\pi)$ is less important at $U = 0.8U_c$ and $0.4U_c$. For the model of $x = 0.5$ in the RPA, we found that $\lambda_{\text{max}}^{\text{S}}(\mathbf{q})^{-1}$ at $\mathbf{q} = (0, 0)$ touches zero at $U = U_c = 0.751$, which is smaller than for the model of $x = 2$, and that there are two main peaks in $\lambda_{\text{max}}^{\text{S}}(\mathbf{q})^{-1}$ at $\mathbf{q} = (0, 0)$ and $\mathbf{q} \sim (0.797\pi, 0)$ and a secondary peak at $\mathbf{q} \sim (\pi, 0.125\pi)$. In contrast to the case of $x = 2$, all the peaks in $\lambda_{\text{max}}^{\text{S}}(\mathbf{q})^{-1}$ arise from the corresponding susceptibilities for the d_{xy} orbital. We also found that $\chi^{\text{S}}(\mathbf{q}, 0)$ at $\mathbf{q} = (0, 0)$ and $\mathbf{q} \sim (\pi, 0.125\pi)$ are dominant at $U = 0.8U_c$, while $\chi^{\text{S}}(\mathbf{q}, 0)$ at $\mathbf{q} = (0, 0)$, $\mathbf{q} \sim (0.797\pi, 0)$, and $(\pi, 0.125\pi)$ are nearly same at $U = 0.4U_c$. The values of $\chi^{\text{S}}(\mathbf{q}, 0)$ along $(0, 0) \rightarrow (\pi, 0)$ are larger than along $(0, 0) \rightarrow (\pi/2, \pi/2)$. Furthermore, we found that the peaks in $\lambda_{\text{max}}^{\text{S}}(\mathbf{q})^{-1}$ for the model of $x = 0.5$ are less sharp than for the model of $x = 2$. These less sharp peaks and the smaller value of U_c will lead to a larger effective mass for the model of $x = 0.5$ than for the model of $x = 2$.

Second, to analyze the effects of the vHs for the d_{xy} orbital, we compared the results at $J_H = U/6$ for the special model with those for the model of $x = 0.5$. In the absence of interactions, we found the larger increase of the noninteracting susceptibility for the d_{xy} orbital and the smaller shifts of the IC peak for the $d_{xz/yz}$ and d_{xy} orbitals towards $\mathbf{q} = (\pi, \pi)$ and $(\pi, 0)$ in the special model. The former is due to the larger increase of the DOS for the d_{xy} orbital near the Fermi level, and the latter is due to the smaller value of $\Delta_{t_{2g}}$. In the presence of interactions, we found that the value of U_c , where $\lambda_{\text{max}}^{\text{S}}(\mathbf{q})^{-1}$ at $\mathbf{q} = (0, 0)$ touches zero, is smaller for the special model than for the model of $x = 0.5$, and that there is a main peak at $\mathbf{q} = (0, 0)$ and there is a secondary peak at $\mathbf{q} \sim (0.703\pi, 0)$; the latter peak corresponds to the peak at $\mathbf{q} \sim (0.797\pi, 0)$ for the model of $x = 0.5$. We also found that all the peaks in $\lambda_{\text{max}}^{\text{S}}(\mathbf{q})^{-1}$ for the special model are slightly sharper than for the model of $x = 0.5$, and that the competition between the modes of spin fluctuation around $\mathbf{q} = (0, 0)$ and $\mathbf{q} \sim (\pi, 0)$ is weaker for the special model. Furthermore, we found that all the enhanced modes in $\lambda_{\text{max}}^{\text{S}}(\mathbf{q})^{-1}$ arise from the corresponding fluctuations for the d_{xy} orbital, and that the dominant contributions to the static susceptibility for a spin sector arise from those for the d_{xy} orbital around $\mathbf{q} = (0, 0)$ and $\mathbf{q} \sim (\pi, 0)$; these results are qualitatively

the same as those for the model of $x = 0.5$.

Third, we analyzed the J_H dependencies of the static susceptibilities for the models of $x = 2$ and 0.5 , and the special model. For all these models, we found that the dominant wave vectors of the static susceptibilities at $J_H = 0$ and $U/4$ are the same as those at $J_H = U/6$, that the increase of J_H/U leads to the decrease of U_c , and that the static susceptibility for a charge sector is enhanced only at $J_H = 0$. In addition to these, we found for the model of $x = 2$ that the increase of J_H/U enhances the IC AF spin fluctuations at $\mathbf{q} \sim (0.688\pi, 0.688\pi)$ and $(\pi, 0.656\pi)$, and that the former IC AF spin fluctuation is strongest for $J_H \geq U/6$ at $U = 0.8U_c \sim 0.78$; these modes correspond to the secondary peaks in $\lambda_{\max}^S(\mathbf{q})^{-1}$ at $J_H = U/6$. The enhancement of the IC AF spin fluctuation at $\mathbf{q} \sim (0.688\pi, 0.688\pi)$ arises not only from the $d_{xz/yz}$ orbital but also from the d_{xy} orbital. Although the similar results have been obtained in the previous mean-field study²² for $x = 2$, we think that a set of the parameters used in this study is more realistic. In contrast to the case of $x = 2$, the increase of J_H/U leads to a nearly uniform enhancement of $\chi^S(\mathbf{q}, 0)$ for the model of $x = 0.5$ and the special model. This difference is due to the much larger contribution from the d_{xy} orbital than from the $d_{xz/yz}$ orbital in the presence of the rotation of RuO₆ octahedra.

In summary, the analyses in the RPA reveal that the rotation of RuO₆ octahedra leads to the enhancement of several modes of spin fluctuation for the d_{xy} orbital around $\mathbf{q} = (0, 0)$ and $\mathbf{q} \sim (\pi, 0)$. This enhancement arises from the increase of the corresponding susceptibilities for the d_{xy} orbital due to the rotation-induced modifications of the electronic structure for this orbital (i.e., the flattening of the bandwidth and the increase of the DOS near the Fermi level). These analyses also reveal that the location of the vHs for the d_{xy} orbital, which is controlled by substitution of Ca for Sr, is a parameter to control the competition between the modes of spin fluctuation for the d_{xy} orbital around $\mathbf{q} = (0, 0)$ and $\mathbf{q} \sim (\pi, 0)$. We propose that the spin fluctuations for the d_{xy} orbital around $\mathbf{q} = (0, 0)$ and $\mathbf{q} \sim (\pi, 0)$ play an important role in the electronic states around $x = 0.5$ other than the criticality approaching the usual Mott transition where all electrons are localized.

Acknowledgments

The authors would like to thank Y. Yanase for a useful comment about the obtained results and T. Kariyado for useful comments about the numerical calculations.

* Electronic address: arakawa@hosi.phys.s.u-tokyo.ac.jp

- ¹ S. Nakatsuji and Y. Maeno, Phys. Rev. Lett. **84**, 2666 (2000).
- ² S. Nakatsuji and Y. Maeno, Phys. Rev. B **62**, 6458 (2000).
- ³ Y. Maeno, H. Hashimoto, K. Yoshida, S. Nishizaki, T. Fujita, J. G. Bednorz, and F. Lichtenberg, Nature (London) **372**, 532 (1994).
- ⁴ K. Ishida, H. Mukuda, Y. Kitaoka, K. Asayama, Z. Q. Mao, Y. Mori, and Y. Maeno, Nature (London) **396**, 658 (1998).
- ⁵ J. A. Duffy, S. M. Hayden, Y. Maeno, Z. Mao, J. Kulda, and G. J. McIntyre, Phys. Rev. Lett. **85**, 5412 (2000).
- ⁶ S. Nakatsuji, D. Hall, L. Balicas, Z. Fisk, K. Sugahara, M. Yoshioka, and Y. Maeno, Phys. Rev. Lett. **90**, 137202 (2003).
- ⁷ S. Nakatsuji, S. Ikeda, and Y. Maeno, J. Phys. Soc. Jpn. **66**, 1868 (1997).
- ⁸ N. Arakawa and M. Ogata, Phys. Rev. B **86**, 125126 (2012).
- ⁹ A. P. Mackenzie, S. R. Julian, A. J. Diver, G. J. McMullan, M. P. Ray, G. G. Lonzarich, Y. Maeno, S. Nishizaki, and T. Fujita, Phys. Rev. Lett. **76**, 3786 (1996).
- ¹⁰ S.-C. Wang, H.-B. Yang, A. K. P. Sekharan, S. Souma, H. Matsui, T. Sato, T. Takahashi, C. Lu, J. Zhang, R. Jin, D. Mandrus, E. W. Plummer, Z. Wang, and H. Ding, Phys. Rev. Lett. **93**, 177007 (2004).
- ¹¹ N. Arakawa and M. Ogata, accepted for publication in J. Korean Phys. Soc. for proceedings of the 19th International Conference on Magnetism with SCES 2012.
- ¹² T. Oguchi, J. Phys. Soc. Jpn. **78**, 044702 (2009).
- ¹³ H. Ehrenreich and M. H. Cohen, Phys. Rev. **115**, 786

- (1959).
- ¹⁴ T. Izuyama, D.-J. Kim and R. Kubo, J. Phys. Soc. Jpn. **18**, 1025 (1963).
- ¹⁵ T. Kariyado, Master thesis, The University of Tokyo (2008).
- ¹⁶ H. Tsunetsugu, J. Phys. Soc. Jpn. **71**, 1844 (2002).
- ¹⁷ Y. Sidis, M. Braden, P. Bourges, B. Hennion, S. NishiZaki, Y. Maeno, and Y. Mori, Phys. Rev. Lett. **83**, 3320 (1999).
- ¹⁸ K. Ishida, Y. Minami, Y. Kitaoka, S. Nakatsuji, N. Kikugawa, and Y. Maeno, Phys. Rev. B **67**, 214412 (2003).
- ¹⁹ O. Friedt, P. Steffens, M. Braden, Y. Sidis, S. Nakatsuji, and Y. Maeno, Phys. Rev. Lett. **93**, 147404 (2004).
- ²⁰ P. Steffens, O. Friedt, Y. Sidis, P. Link, J. Kulda, K. Schmalzl, S. Nakatsuji, and M. Braden, Phys. Rev. B **83**, 054429 (2011).
- ²¹ T. Takimoto, Phys. Rev. B **62**, R14641 (2000).
- ²² T. Nomura and K. Yamada, J. Phys. Soc. Jpn. **69**, 1856 (2000).
- ²³ N. F. Berk and J. R. Schrieffer, Phys. Rev. Lett. **17**, 433 (1966).
- ²⁴ S. Doniach and S. Engelsberg, Phys. Rev. Lett. **17**, 750 (1966).
- ²⁵ T. Moriya, Phys. Rev. Lett. **24**, 1433 (1970).
- ²⁶ Y. Yamashita and K. Ueda, Phys. Rev. B **67**, 195107 (2003).
- ²⁷ J. Mravlje, M. Aichhorn, T. Miyake, K. Haule, G. Kotliar, and A. Georges, Phys. Rev. Lett. **106**, 096401 (2011).
- ²⁸ T. Moriya and A. Kawabata, J. Phys. Soc. Jpn. **34**, 639 (1973).
- ²⁹ H. Hasegawa and T. Moriya, J. Phys. Soc. Jpn. **36**, 1542 (1974).

- ³⁰ T. Moriya, *J. Magn. Magn. Mater.* **14**, 1 (1979).
- ³¹ T. Moriya, *Prog. Theor. Phys. Suppl.* **69**, 323 (1980).
- ³² Y. Yanase and M. Ogata, *J. Phys. Soc. Jpn.* **72**, 673 (2003).
- ³³ N. Arakawa and M. Ogata, 2012 Fall Meeting of the Physical Society of Japan, 2012, 18aGB-9.
- ³⁴ Z. Fang and K. Terakura, *Phys. Rev. B* **64**, 020509(R) (2001).
- ³⁵ E. Ko, B. J. Kim, C. Kim, and H. J. Choi, *Phys. Rev. Lett.* **98**, 226401 (2007).
- ³⁶ K. Ishida, H. Mukuda, Y. Minami, Y. Kitaoka, Z. Q. Mao, H. Fukazawa, and Y. Maeno, *Phys. Rev. B* **64**, 100501(R) (2001).
- ³⁷ J. P. Carlo, T. Goko, I. M. Gat-Malureanu, P. L. Russo, A. T. Savici, A. A. Aczel, G. J. MacDougall, J. A. Rodriguez, T. J. Williams, G. M. Luke, C. R. Wiebe, Y. Yoshida, S. Nakatsuji, Y. Maeno, T. Taniguchi, and Y. J. Uemura, *Nat. Mater.* **11**, 323 (2012).
- ³⁸ L. M. Galvin, R. S. Perry, A. W. Tyler, A. P. Mackenzie, S. Nakatsuji, and Y. Maeno, *Phys. Rev. B* **63**, 161102(R) (2001).
- ³⁹ O. Friedt, M. Braden, G. André, P. Adelman, S. Nakatsuji, and Y. Maeno, *Phys. Rev. B* **63**, 174432 (2001).
- ⁴⁰ A. Gukasov, M. Braden, R. J. Papoular, S. Nakatsuji, and Y. Maeno, *Phys. Rev. Lett.* **89**, 087202 (2002).
- ⁴¹ S. Nakatsuji and Y. Maeno, *J. Low Temp. Phys.* **117**, 1593 (1999).
- ⁴² J. S. Lee, Y. S. Lee, T. W. Noh, S.-J. Oh, J. Yu, S. Nakatsuji, H. Fukazawa, and Y. Maeno, *Phys. Rev. Lett.* **89**, 257402 (2002).